JOURNAL OF CATALYSIS **180,** 245–257 (1998)
ARTICLE NO. CA982268

Kinetics of Carbon–NO Reaction Studied by Scanning Tunneling Microscopy on the Basal Plane of Graphite

Ning Chen,* Ralph T. Yang,*,[1] and Rachel S. Goldman†

*Department of Chemical Engineering, †Department of Material Science and Engineering, University of Michigan, Ann Arbor, Michigan 48109

Received May 29, 1998; revised August 26, 1998; accepted August 27, 1998

The carbon–NO reaction was studied by scanning tunneling microscopy (STM) on the basal plane of graphite (HOPG) samples in a wide temperature range of 500–900°C. Monolayer etch pits, multilayer (deep) etch pits, and nascent etch pits were observed for the graphite–NO reaction in different reaction temperature regimes. The formation of deep pits and nascent pits became prevalent at higher temperatures, e.g., 850°C with 1% NO. No temperature "break" point in the Arrhenius plot of the turnover frequency (TOF) rates was observed. The activation energy for the graphite–NO reaction was 132 kJ/mol, which was relatively low compared to literature data. Careful analysis of basal plane STM features revealed that the often-reported (by others) temperature "break" point in the Arrhenius plot was caused by the contribution of NO basal plane c-attack in the higher temperature range, which forms nascent etch pits and deep pits. The formation of nascent and deep pits with higher activation energies (than that for monolayer etching) contributed to the higher apparent activation energy in the high temperature range. In global rate measurements for the NO-carbon reaction, it is not possible to distinguish between the monolayer etching process and basal plane c-attack. The TOF measured by the STM method were true intrinsic rates for edge site monolayer recession. For the NO-graphite reaction, the reaction is first order with respect to NO. The NO–graphite reaction is at least 15 times faster than the O_2-graphite reaction. The NO-graphite and N_2O–graphite reactions might have the same rate-limiting step in the low temperature range, but have different rate-limiting steps in the high temperature range.

INTRODUCTION

The carbon gasification reactions, i.e., the reactions of $C + O_2$, $C + CO_2$, $C + H_2O$, $C + H_2$, and $C + NO$, have been studied extensively (1–14). The importance of these reactions in combustion processes, catalysis and metallurgy requires a fundamental understanding for these reactions. Among these reactions, the $C + CO_2$ reaction is the best understood one. The $C + O_2$, $C + H_2O$, and $C + H_2$ are relatively well understood. The $C + NO$ reaction is the least understood reaction. Many experimental techniques have been used in the studies of carbon gasification reactions. TPD (temperature-programmed desorption), TGA (thermogravimetric analysis), and TK (transient kinetics) are among them. For single-crystal graphite, gold-decoration TEM (transmission electron microscopy) was developed (2, 15), which allows one to investigate the gasification reactions taking place on the graphite basal plane through the formation of etch pits and channels by imaging the gold particles nucleated on the edges. A basic understanding on uncatalyzed and catalyzed carbon gasification has been obtained by the TEM technique (16–23). More recently, STM (scanning tunneling microscopy) was used to study the graphite basal plane reactions through surface topographic images (24–27), which included monolayer etch pits and channeling.

The $C + NO$ reaction is attracting wide interests because of its environmental ramifications. The emission of nitrogen oxides (NO and N_2O) from combustion processes is the cause for several environmental problems, including the formation of acid rain, stratospheric ozone depletion, and the "greenhouse" effect. Moreover, localized nitric oxides from energy generation power plants can cause respiratory system problems (28, 29). It was found that the use of carbon with proper catalysts to convert nitric oxides to CO_2 and N_2 in the combustion process is a possible approach for the reduction of nitrogen oxides (30). However, the $C + NO$ reaction is studied much less than the other carbon gasification reactions, and its understanding is in a primitive stage. There are no satisfactory kinetic models for the reaction, and much less is known about the reaction mechanism. Several groups have investigated the $C + NO$ reaction (31–52). There are a few excellent reviews for the $C + NO$ reaction (53, 54). The general conclusions on the $C + NO$ reaction are: (a) there is a very poor correlation between all available experimental kinetic data, and the situation is the same even for graphite samples, the most highly ordered form of carbon; (b) there is a temperature "break" point in the Arrhenius plot, wherein the activation energy of the reaction increases from 15–30 kcal/mol (or 63–125 kJ/mol) in the lower temperature range to 40 kcal/mol in the higher

[1] Address all correspondence to R. T. Yang. E-mail: yang@engin.umich.edu.

0021-9517/98 $25.00

temperature range (below about 650°C); but at the same time, many investigators did not observe such a "break"; (c) it is a first-order reaction with respect to NO concentration; (d) graphite samples generally exhibited low reactivities and high activation energies, although a large range of activation energies was observed. Chu and Schmidt studied the intrinsic kinetics of the reactions between graphite and NO_x (i.e., NO, N_2O, and NO_2) by the STM technique, and important conclusions have been reached (25, 35). However, the highest temperature in their study was 650°C; hence the important question on the temperature break could not be addressed.

In this work, we measured the intrinsic kinetics of the $C + NO_x$ reactions in the temperature range 500–900°C, using the STM technique. From the rate results, we will address several important issues on the kinetics, in particular, on the temperature break. An explanation is given for the origin of the "break" point that is observed in the global kinetics.

EXPERIMENTAL

Materials

HOPG (highly oriented pyrolytic graphite), grade ZYD, from Union Carbide was used as the carbon sample. Because of the high purity of this graphite sample, it is possible to avoid involvement of any catalytic effects, which would be caused by impurities in the sample. The HOPG sample is composed of numerous graphite single crystals. The joining points of these single crystals form mosaic angles. The HOPG grade code indicates the mosaic angles, and there is no difference of purity between different grades. The ZYD sample had a mosaic angle of about 2°. A detailed description of the HOPG is given elsewhere (67). Helium was ultra high purity (from Matheson) and was subjected to further purification to remove traces of O_2 by passing through copper turnings at 550°C, since the presence of O_2 would enhance the etching rates. NO and N_2O (from Matheson) were premixed with 1% concentration and used without further treatment. O_2 was high purity grade (from Matheson) and mixed with helium to obtain desired concentrations through a gas blending system.

Gasification Reaction

The HOPG sample was cut and cleaved into small and thin pieces to fit into the STM sample puck size. The small HOPG sample pieces were further peeled with Scotch tape to expose the fresh surface. Then samples were placed on a sapphire plate held in an alumina combustion boat. The boat was placed in a quartz tube furnace reactor. Prior to the gasification reaction, it was necessary to degas the basal plane in inert gas (helium was used) at 500°C overnight (2) in order to remove surface oxide and expose the active surface. After degassing, the temperature was raised to the desired reaction temperature and the gas was switched to desired reaction gases. After a certain time of reaction, the reaction gases were switched back to helium and the temperature was allowed to drop to ambient temperature quickly in order to reduce any postreaction.

STM Experiment

The reacted samples were glued to the STM sample puck with conducting silver paint. The STM tips were prepared as follows: first a piece of tungsten wire was cut to pieces using scissors to form tips, and the cut tips were subjected to a electrochemical polishing procedure under a 10-V constant voltage in 1 *N* NaOH solution (55), and finally, the polished tips were electrochemically etched under the same conditions as above but on a high magnification optical microscope to further sharpen the tips (56). The STM experiments were carried out on a NanoScope III scanning probe microscope (from Digital Instruments) under ambient conditions. The STM was operated in the constant current mode; this would give the result in height as the *z*-parameter, i.e., the *z*-distance perpendicular to the basal plane. The general conditions used in this study were: setpoint = 2.0 nA; bias = 2.0 V; scan rate = 1.0 Hz; integral gain = 3.0; proportional gain = 2.0. The images shown in the paper were filtered by lowpass filtering and/or fast Fourier transform to obtain clearer images. Care was taken to ensure that no information was lost during filtering of the images.

The surfaces were first scanned randomly at $100 \times 100\ \mu m^2$ on about 10 different regions to find featured areas. These featured spots were further scanned with a lower *z*-range and a slower scan rate to obtain clear images with high resolution in both plane (*x*-*y*) direction and the *z*-direction. The etching rates were measured from average diameters over several of the largest etch pits on the same sample.

RESULTS AND DISCUSSION

Fundamental Consideration

Anisotropy on the graphite surface refers to the orders of magnitude higher reactivities on the edge carbon atoms, i.e., on the zigzag or armchair faces, than on the basal plane. This anisotropy is caused by the free sp^2 electron on the edge atoms. When the basal plane of graphite sample is exposed to a reactant gas, a single vacancy on the basal plane, which is surrounded by three edge atoms, can be expanded to form an etch pit, and this pit is one atomic layer deep, i.e. 3.35 Å. The graphite gasification reactions take place through this type of edge recession process (2). Therefore, the reaction rate for this process is the intrinsic rate for edge site etch process, and in turn, the study of

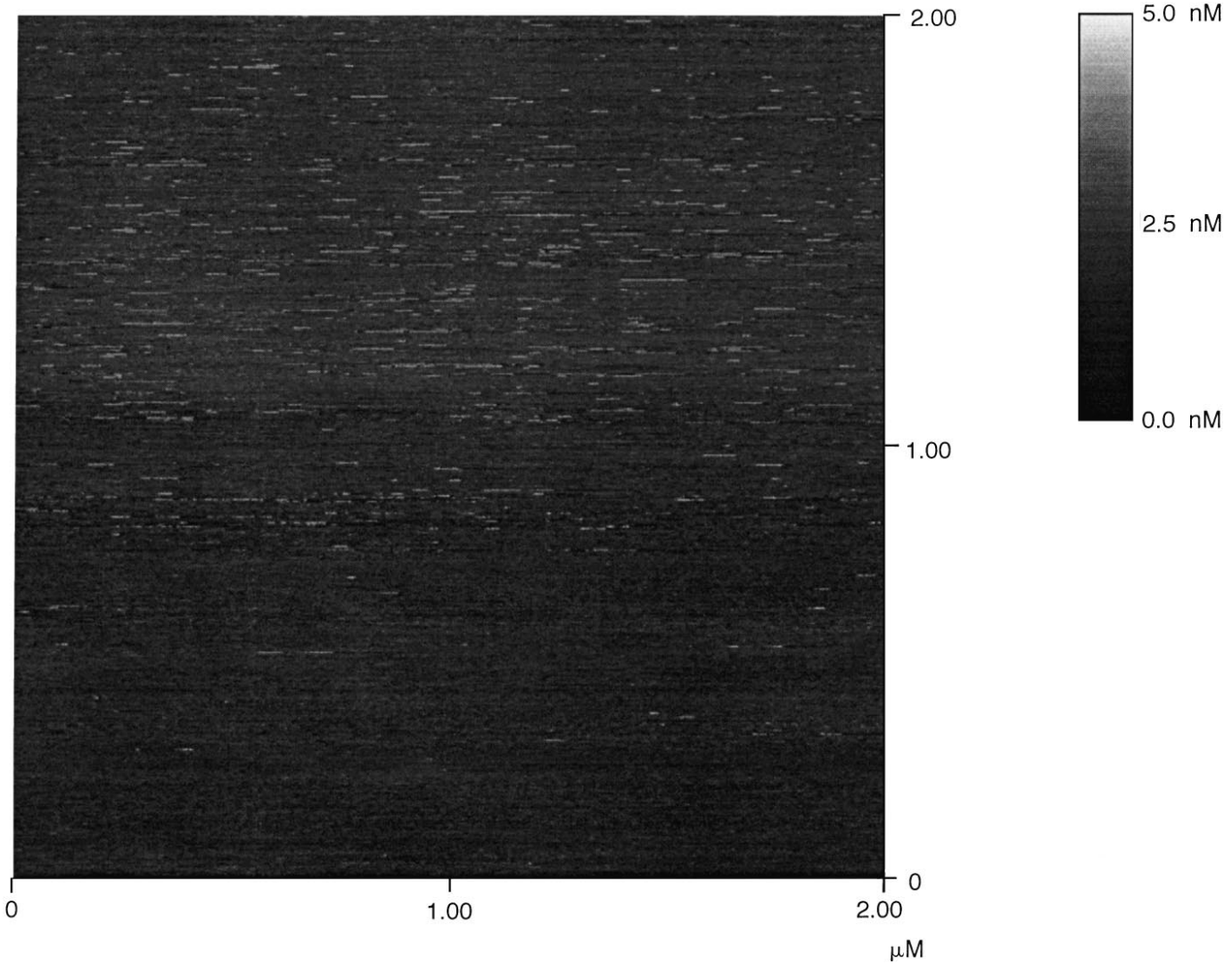

FIG. 1. STM image of blank graphite sample treated under the same conditions as the reaction at 750°C, but without the presence of NO, time = 30 min.

graphite gasification reactions on the basal plane can be used to establish some fundamental kinetic understanding for carbon gasification reactions. The calculation of rate for etch pit expansion, i.e., TOF (turnover frequency), has been well established as Eq. [1] (17, 57),

$$\mathrm{TOF} = \mathrm{rate}\left(\frac{\text{atoms gasified}}{\text{edge atoms} \times \text{s}}\right) = \frac{\rho_{0001}\pi D\, dD/dt}{\rho_{1120}\pi DH}$$
$$= 0.4689\frac{dD}{dt} = kP\exp(-E/RT), \qquad [1]$$

where $\rho_{0001} = 0.377$ carbon atoms/Å^2, $\rho_{1120} = 0.120$ carbon atoms/Å^2, H = monolayer step height = 3.35 Å for graphite, D = diameter of the monolayer pit, t = time of gasification reaction in seconds, k = preexponential factor, E = activation energy, T = reaction temperature in K, and P = partial pressure of reactant. Therefore, the activation energy can be obtained through the slope of the $\ln(\mathrm{TOF}) - 1/T$ plot.

Besides the monolayer etch pit formation, there are other processes that also take place during carbon gasification reactions. The c-attack, or basal plane atom abstraction, causes the formation of nascent pits with smaller diameters. Since the times of birth of these nascent pits are not known, the calculation of rates for these pits would be meaningless. For the C–NO reaction, formation of nascent pits become significant at temperatures higher than 750°C. The contribution by the nascent pit formation to the overall gasification rate increases with temperature. The actual contribution is not measured in this work. In addition, multilayer pits are sometimes observed and are usually caused by the screw dislocation in the graphite crystal where cooperative effects (among adjacent layers) can be involved (2).

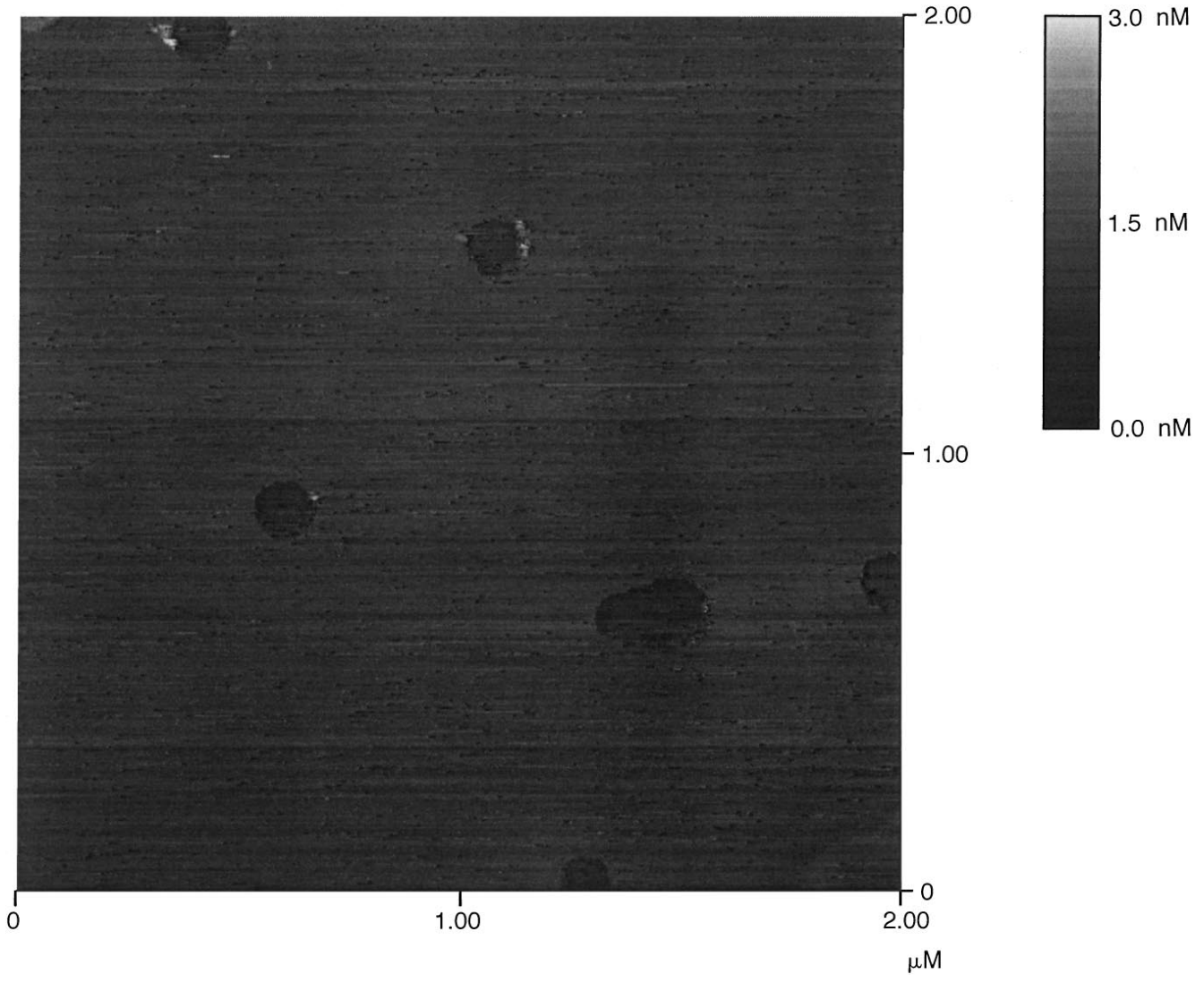

FIG. 2. STM image of graphite sample after reaction with 1% NO at 550°C, time = 120 min.

Etching Process of NO–Graphite Reaction

Figure 1 is an STM image of a blank graphite sample treated in the same run as the reaction at 750°C, but without the presence of NO. The image clearly shows that the sample surface is clean and featureless, indicating that the pretreatment procedure does not produce any surface features.

At 550°C the etch pits were formed through the reaction with 1% NO, as shown in the STM image in Fig. 2. The pits in the image are all circular in shape with approximately the same diameter and are monolayer in depth. These results indicate that the etching process occurred uniformly over the basal plane, as in the case of the graphite–O_2 reaction (2).

Figures 3 and 4 show results from higher temperatures, i.e., 700–750°C, where pits with different diameters were observed. The observation of a variety of sizes indicates that when the reaction temperature was increased, the possibility of a NO c-attack process increased. The NO c-attack results in the formation of nascent pits (2), which have smaller diameters than the original pits since the etching process is delayed until the formation of nascent vacancies by the NO c-attack. The detailed depth profile through section analysis for the pit in Fig. 4 is shown in Fig. 5. It is clearly seen that the etch pit is monolayer deep with 3.39 Å in the *z*-direction (c-axis in the conventional graphite crystal orientation), which is the layer–layer distance of graphite of 3.35 Å. An interesting observation from Figs. 3 and 4 is the formation of double layer pits, one in the right-middle of Fig. 3 and another near the center of Fig. 4. Section analysis in Fig. 6 indicates that the pit on the second layer is also of monolayer depth, based on the second layer (double layer depth from the top layer) with 3.20 Å, see the *b*-*b*′ pair of cursors. This observation is quite common for our sample.

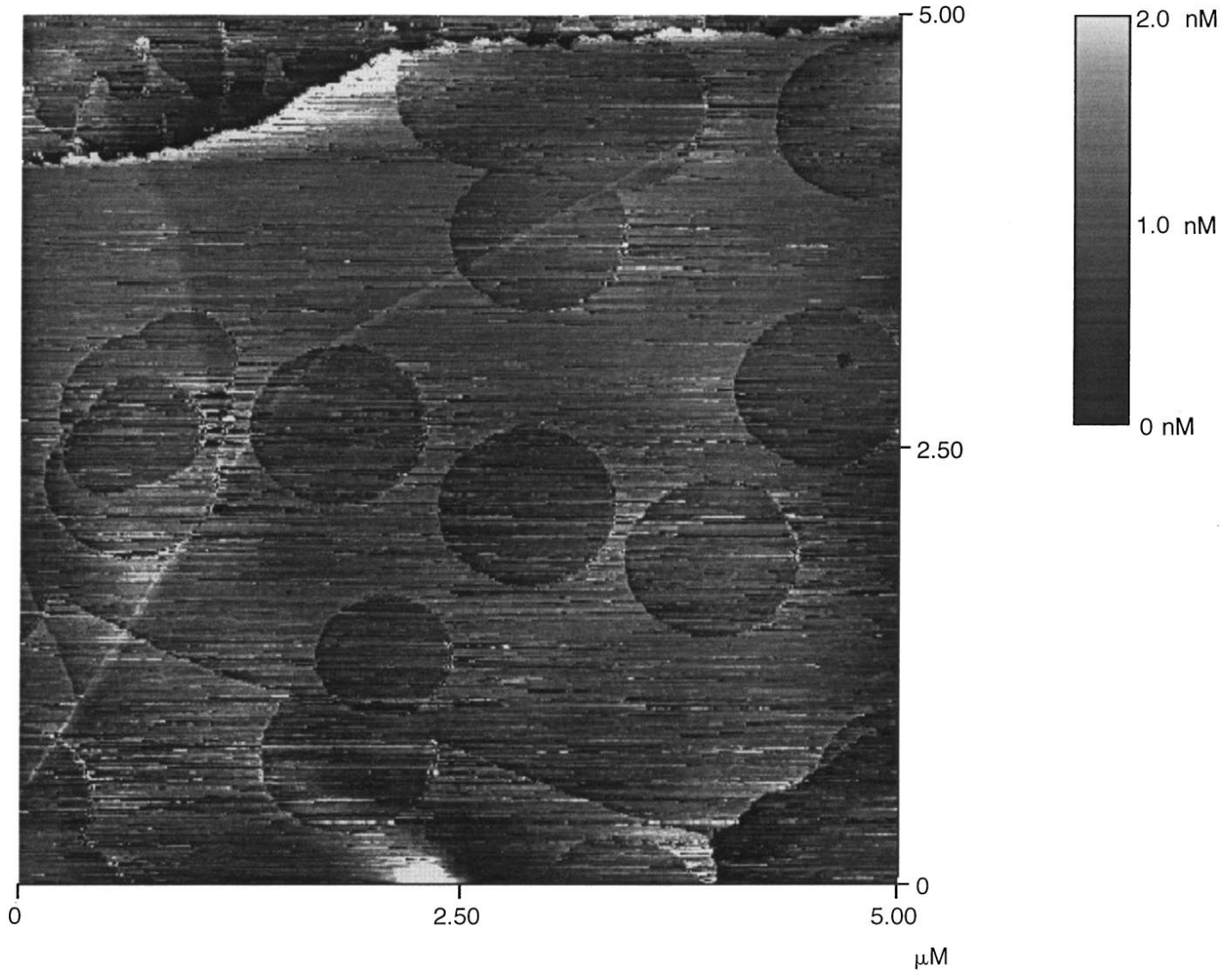

FIG. 3. STM image of graphite sample after reaction with 1% NO at 700°C, time = 45 min.

This double layer pit was developed when the etching of the first layer pit exposes a vacancy on the second layer plane. Usually the double layer pits are tangential to the first layer pits, i.e., they always have the same reaction rate at the point of contact. However, the double layer pits in Fig. 3 are not tangential to the first layer pit; there was some obvious distance between two pits on different layers. The double layer pits apparently resulted from the NO c-attack on the second layer, forming nascent pits on the second layer.

When the reaction temperature was further increased, multilayer pits formed throughout the basal plane, indicating a severe gasification reaction had occurred, both on the basal plane and at the c-axis, resulting in multilayer etching. Figure 7 shows a multilayer pit more than 20 layers deep that was formed at 900°C, and this was a very common observation through our experiment when the temperature was increased to 850°C. The multilayer pit is concentric rather than tangential, indicating that its formation mechanism was different from that for the monolayer pit. The multilayer pit does not have the perfect circular shape of the monolayer pits, although it is generally rounded. Since the catalytic reaction (by catalysts or impurity) should be faster than the noncatalytic one, one should be able to observe the formation of multilayer pit under both high and low temperatures. Since the multilayer pits are observed only at high temperatures, the involvement of catalysts or impurities is ruled out. Another possible explanation for the formation of deep multilayer pit is the existence of screw dislocations within the graphite sample, which were the reactive sites. However, screw dislocations are actually a combination of many vacancies on different layers, and they are much more reactive than a single vacancy under the whole temperature range. Again, since the multilayer pits were not observed at

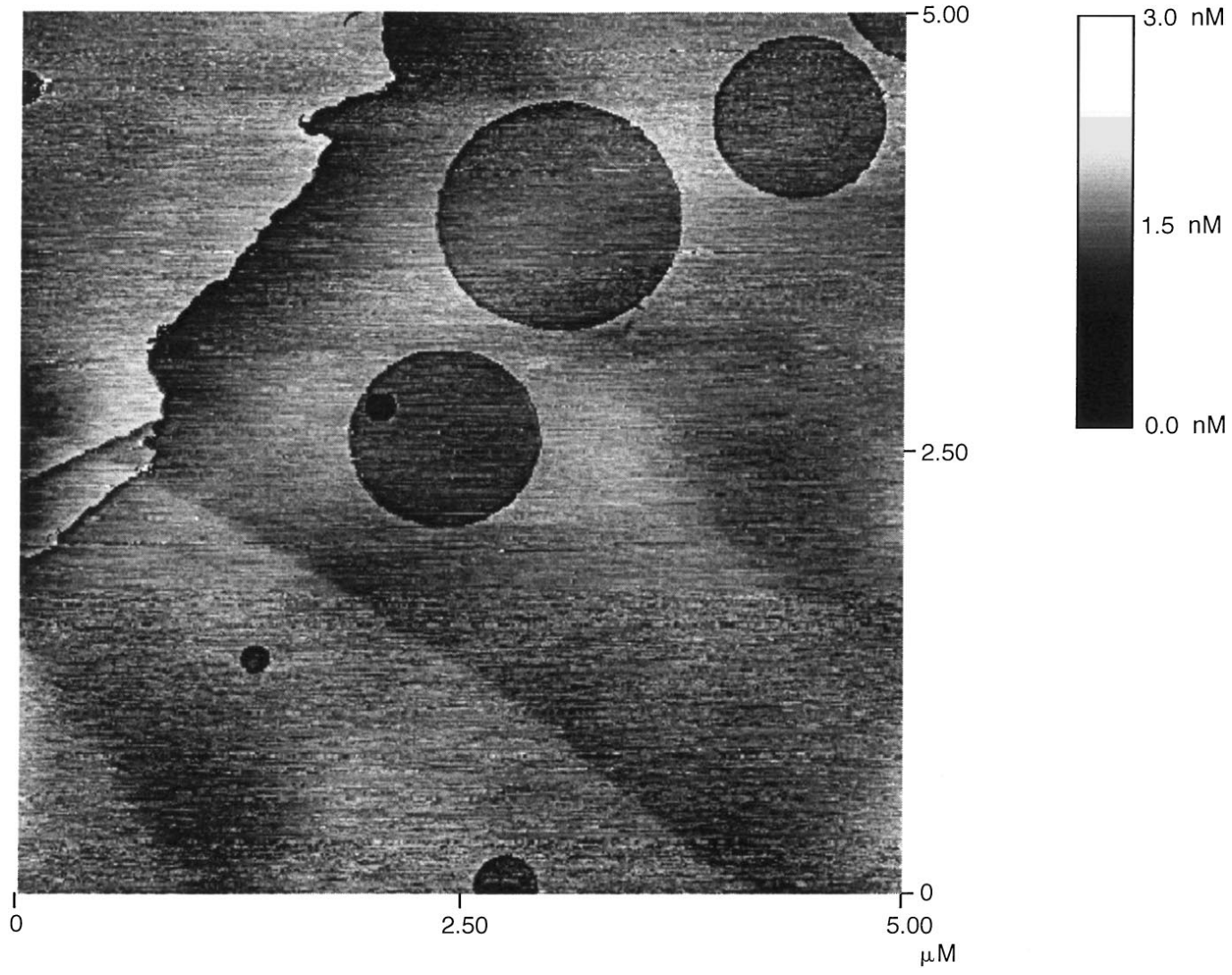

FIG. 4. STM image of graphite sample after reaction with 1% NO at 750°C, time = 30 min.

low temperatures, a mechanism based on screw dislocations is ruled out.

The only plausible explanation for the formation of the deep pits at high temperatures is as follows. We first note that the homogeneous dissociation constants (forming oxygen atoms) are substantially higher for NO than for O_2, H_2O, and CO_2. A comparison of the equilibrium dissociation constants is given in Table 1. The dissociation constants (K) are listed for four reactions: $2NO \rightarrow N_2O + O$; $O_2 \rightarrow O + O$; $H_2O \rightarrow H_2 + O$; and $CO_2 \rightarrow CO + O$. From Table 3, it is seen that the dissociation of NO is much easier than O_2, H_2O, and CO_2. Consequently, more nascent pits on the basal plane are expected from NO since oxygen atoms are responsible for the abstraction of carbon atoms from the basal plane, as we have observed previously (2, 57, 58). Furthermore, dissociation of the oxygen-containing molecules (i.e., NO, O_2, H_2O, and CO_2) is facilitated on the

TABLE 1

Comparison of Homogeneous Dissociation Equilibrium Constants (K)

	K[a]				
T (°C)	$NO \rightarrow O + N$	$2NO \rightarrow N_2O + O$	$O_2 \rightarrow O + O$	$H_2O \rightarrow H_2 + O$	$CO_2 \rightarrow CO + O$
925	1.9×10^{-22}	3.2×10^{-9}	6.2×10^{-16}	1.2×10^{-17}	1.6×10^{-17}
825	5.7×10^{-25}	7.7×10^{-10}	6.1×10^{-18}	3.8×10^{-19}	3.9×10^{-19}
725	5.3×10^{-28}	1.4×10^{-10}	2.4×10^{-20}	6.2×10^{-21}	4.2×10^{-21}
625	1.0×10^{-31}	1.8×10^{-11}	2.8×10^{-23}	3.9×10^{-23}	1.8×10^{-23}
525	2.5×10^{-36}	1.3×10^{-12}	6.2×10^{-27}	7.4×10^{-26}	1.7×10^{-26}
425	2.8×10^{-42}	5.0×10^{-14}	1.3×10^{-31}	2.4×10^{-29}	2.5×10^{-30}

[a] Calculated from free energies of formation data, JANAF Thermochemical Tables, 2nd ed., NSRDS. National Bureau of Standards, Washington, DC, 1971.

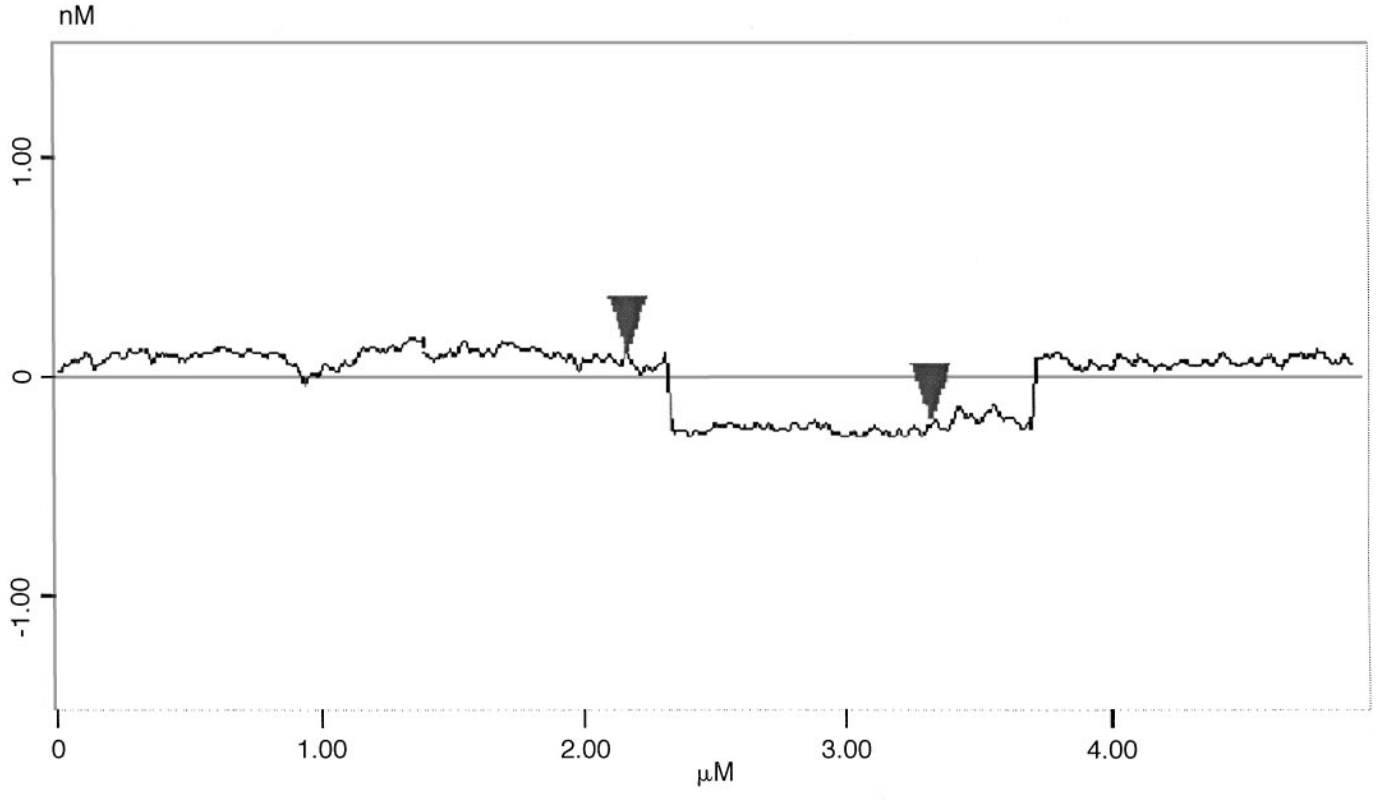

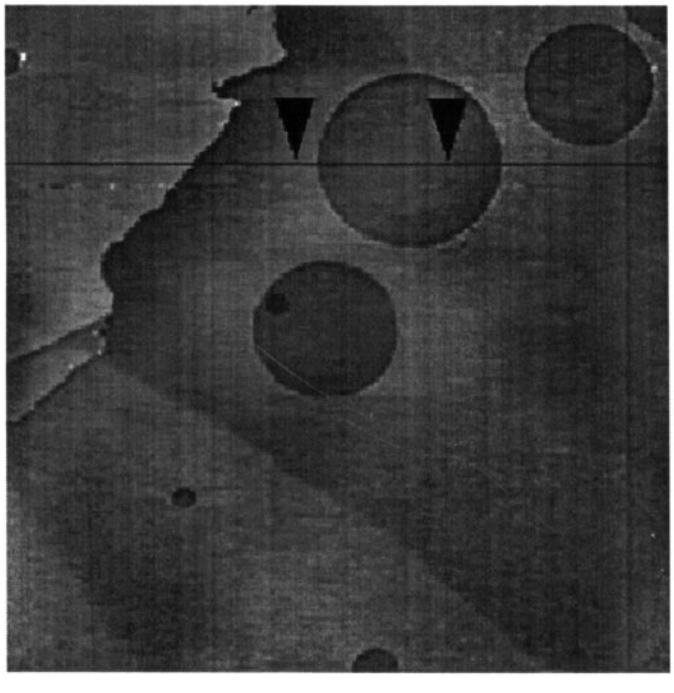

Horiz distance (L)	1.152 μM
Vert distance	0.339
Angle	0.017
Horiz distance	
Vert distance	
Angle	
Horiz distance	
Vert distance	
Angle	
Spectral period	DC
Spectral freq	0 Hz
Spectral RMS amp	0.0009 nM

FIG. 5. Section analysis for STM results from Fig. 4, showing etch pit with monolayer depth of 3.39 Å.

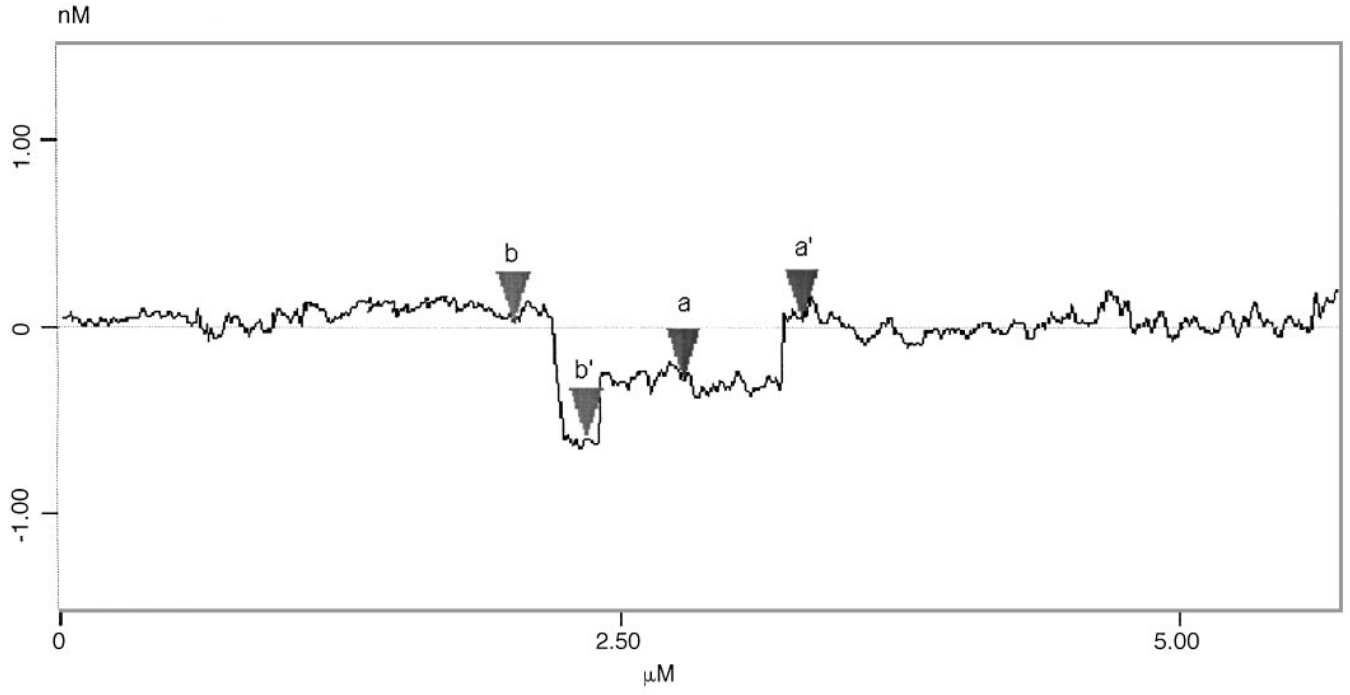

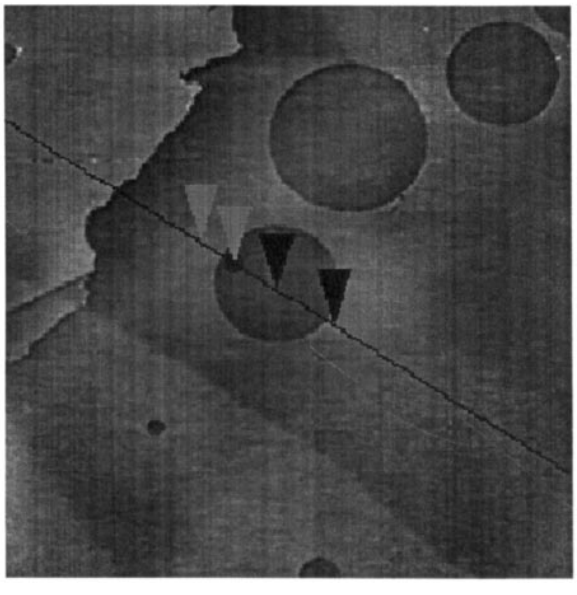

Horiz distance (L)	556.64 nM
Vert distance	0.347 nM
Angle	0.036 deg
Horiz distance	322.27 nM
Vert distance	0.667 nM
Angle	0.119 deg
Horiz distance	
Vert distance	
Angle	
Spectral period	DC
Spectral freq	0 Hz
Spectral RMS amp	0.015 nM

FIG. 6. Section analysis for STM results from Fig. 4, showing double layer etch pit depth of 3.20 Å corresponding to the second layer or a total depth of 6.67 Å from the first layer.

edge carbon atoms, i.e., active sites, via

$$C(\text{edge}) + NO \rightarrow C(O) + N_2O. \quad [2]$$

The dissociation rate constants on active sites of carbon for H_2O and CO_2 have been carefully measured by Walker and co-workers (59, 60). The rates for NO dissociation on the carbon active sites are not known but are undoubtedly higher than for the other gases. Hence, it is expected that there is a high concentration of oxygen atoms within the etch pit when the temperature is high. The oxygen atoms generate new vacancies and a new pit within the first pit. The process repeats itself and successive inner pits are thus

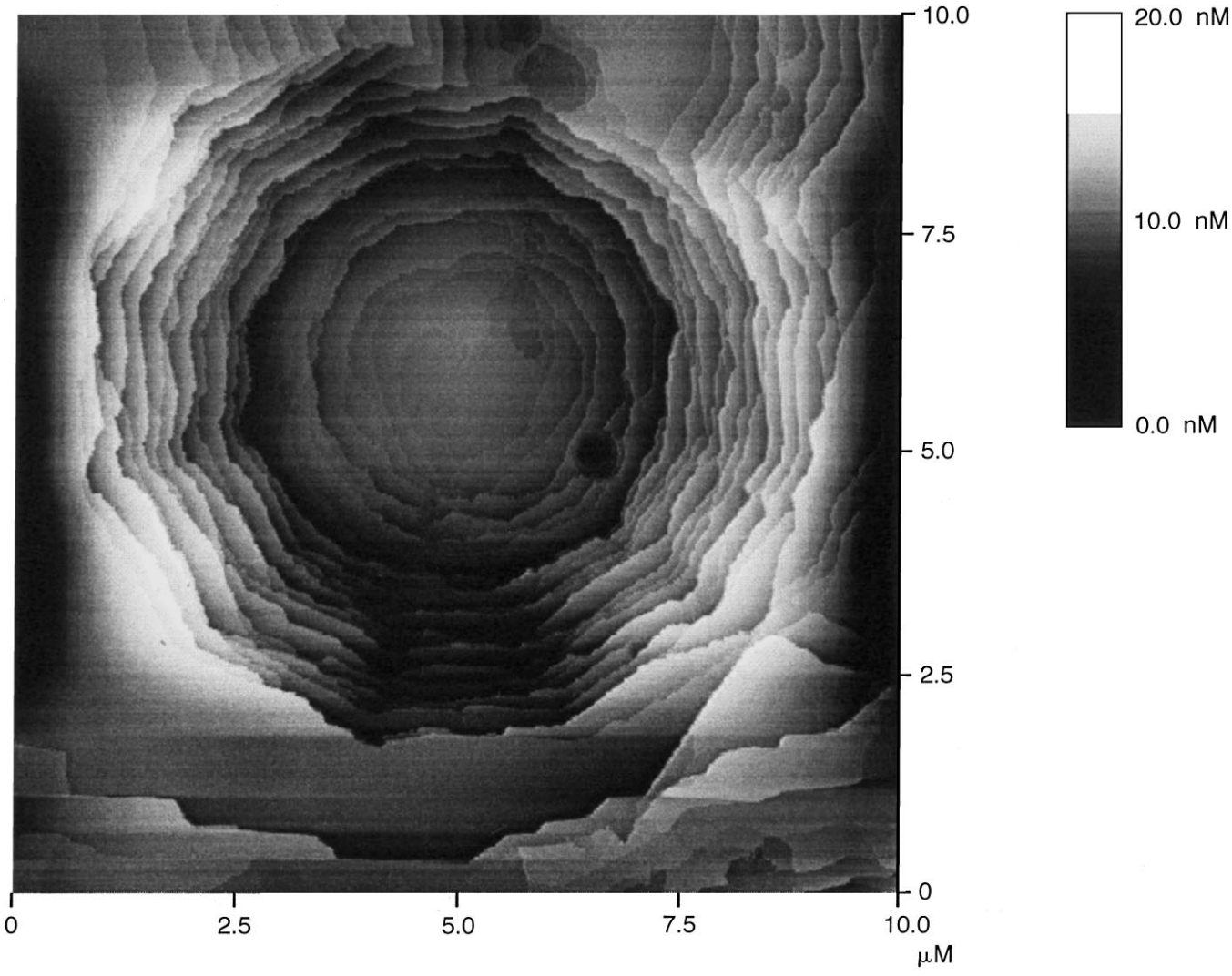

FIG. 7. STM image of graphite sample after reaction with 1% NO at 900°C, showing a multilayer pit with over 20 layers and a tapered pit, time = 5 min.

formed. This process results in the deep pit observed in this work. It is important to note that these deep pits are prevalent at high temperatures for the C + NO reaction, and it (i.e., deep pitting) clearly contributes significantly to the global rate of gasification. The mobility of oxygen on the basal plane (16, 17) would facilitate the formation of deep pits. The cooperative effects on the multilayer edges (i.e., the recession rates can be significantly higher on the multilayer edges than that on the single-layer edge) (61, 62) would further increase the gasification rates.

Finally, Fig. 8 presents an image of graphite gasified with 5% NO at 600°C, which is five times higher in NO concentration than all of the other runs. The calculated TOF for this run is about 1.51 s^{-1}, exactly five times of 1% NO run. (The data are listed in Tables 2 and 3). This result indicates that the graphite gasification with NO is a first-order reaction with respect to NO concentration.

It is important to compare our kinetic data to the available literature data of Chu and Schmidt (25). Under the same reaction conditions, i.e., 600°C and 1% NO, our rate (TOF) is 0.28 1/s with an activation energy of 132.3 kJ/mol. From their data, estimated from the Arrhenius plot, the TOF is about 1.0 1/s, and their activation energy for monolayer etching is 91 ± 3 kJ/mol. The narrow temperature range in their report (from 500°C to 650°C) might affect the accuracy of their activation energy data. The difference between the TOFs is noticeable, but is not thought to be very significant, since for the same TOF, the discrepancy in temperature would be about 50°C. Our TOF data for the HOPG-O_2 reaction from a parallel experiment is very well correlated with the TOF data for Ticoderoga graphite–O_2 reaction by gold-decoration TEM (2). Therefore, it is reasonable to believe that our TOF data for HOPG–NO reaction is accurate. The pretreatment procedure, i.e.,

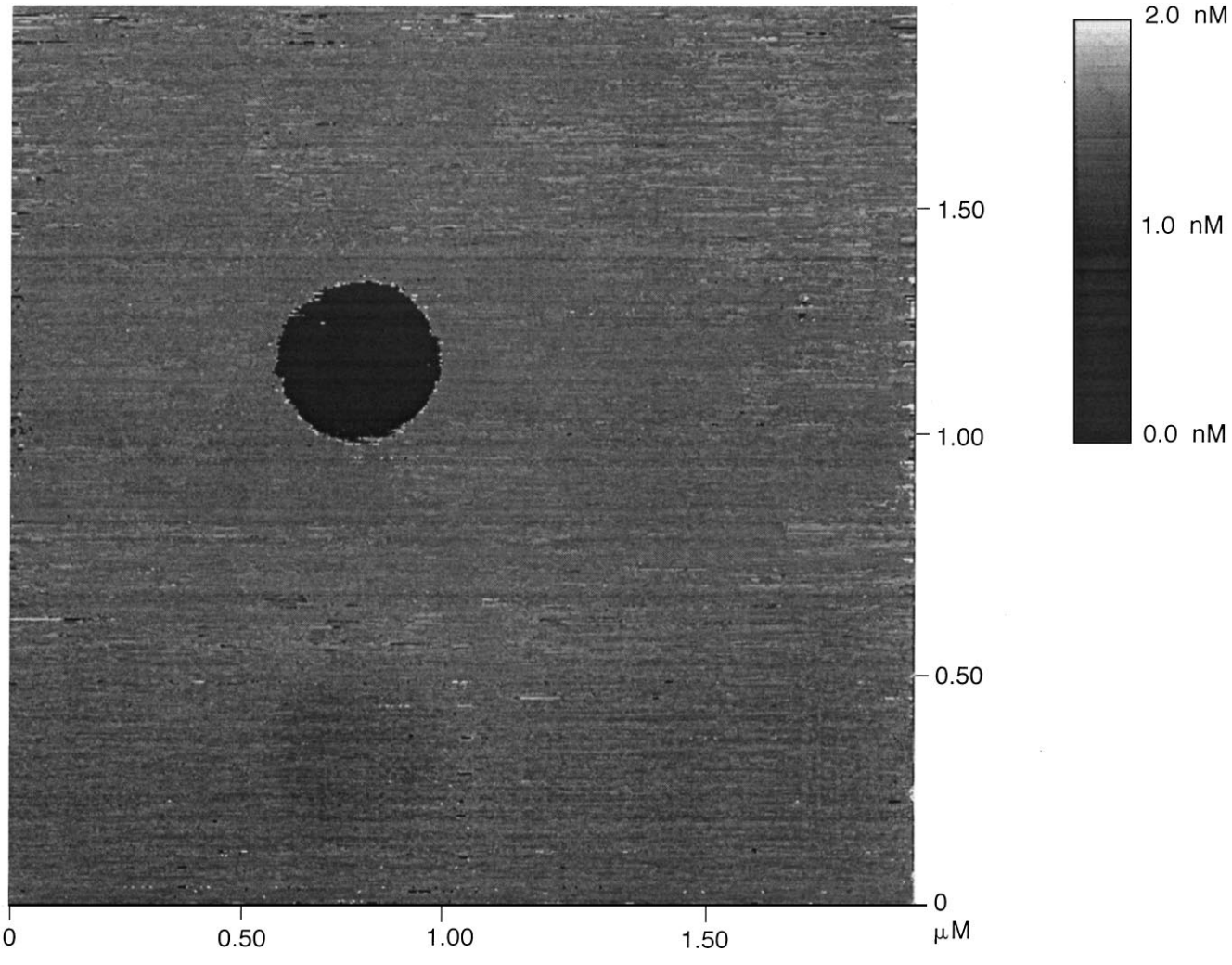

FIG. 8. STM image of graphite sample after reaction with 5% NO at 600°C, time = 20 min.

degassing and purification by high purity grade helium (carrier gas), as well as reaction conditions (i.e., temperature and gas sequencing) may play a significant role if they are well controlled.

Kinetic Behavior of NO–Graphite Reaction

The observation of a "break" point in the Arrhenius plot with two activation energies for the NO–carbon reaction

TABLE 2

Summary of TOF (1/s) for the Graphite–NO Reaction with 1% NO in He at 1 atm Measured by STM

T (°C)	Time (s)	1000/T (1/K)	TOF1	TOF2	TOF3	TOF4	TOF5	TOF6
900	300	0.85	17.52	20.61	27.32	53.27		60.44
850	600	0.89	13.28	15.19	17.63			18.09
800	1200	0.93	6.91	7.27	8.17			9.67
750	1800	0.98	2.87					3.77
700	2700	1.03	1.21	1.50	1.51	1.58	1.58	1.67
650	3600	1.08	0.65					1.00
600	5400	1.15	0.28	0.28				0.31
550	7200	1.22	0.082	0.086	0.089	0.089	0.093	0.099
500	10800	1.29	0.033	0.036	0.037	0.037		0.042

TABLE 3

Summary of TOF (1/s) for Gas–Graphite Reactions under Different Reaction Conditions

	T (°C)	500	550	600	650	700	750	800	850	900
Sample	Reactant									
HOPG	1% NO	0.04	0.10	0.28	0.85	1.44	3.51	9.98	18.0	32.9
HOPG	5% NO			1.51						
HOPG	1% N_2O			0.29				17.3		
HOPG	20% O_2						4.46		17.3	
Ticonderoga[a]	36% O_2				1.1	3.0	7.1	15.8		

[a] Natural graphite single crystal (2).

has been reported by many sources in the literature. However, there is also evidence for the absence of the "break" point, and the activation energies with no "break" point generally were low, as has been discussed in recent reviews (53, 54). This "break" point in the Arrhenius plot is not well understood, although the transition temperature indicates a change in mechanism, and the NO–carbon reaction in two temperature regimes can be controlled or dominated by different elementary processes with different activation energies (53, 54).

As discussed above, because of the unknown history of nascent etch pits, the etch pit diameter measurement should be carried out only on the original pits. To achieve this goal, we first scanned the surface on a very large area, 100 × 100 μm^2. Then certain area were scanned and only the diameters of the largest pits, i.e., the original pits, were measured. Furthermore, the diameter versus time data (hence, TOF) for different pits were collected to generate the error bars as shown in Fig. 9. Table 2 lists primary (average) data from nine runs at different temperatures. Figure 9 presents the temperature dependence of the data in Table 2.

According to our experimental procedure, the measured TOF rates should be the true intrinsic rates for edge site reaction. From this analysis, we find an activation energy of 132.3 kJ/mol (31.6 kcal/mol), which would classify our NO–graphite reaction in the group of the lowest reactivity and the highest activation energy among NO–carbon reactions reported in the literature. Not unexpectedly, this result

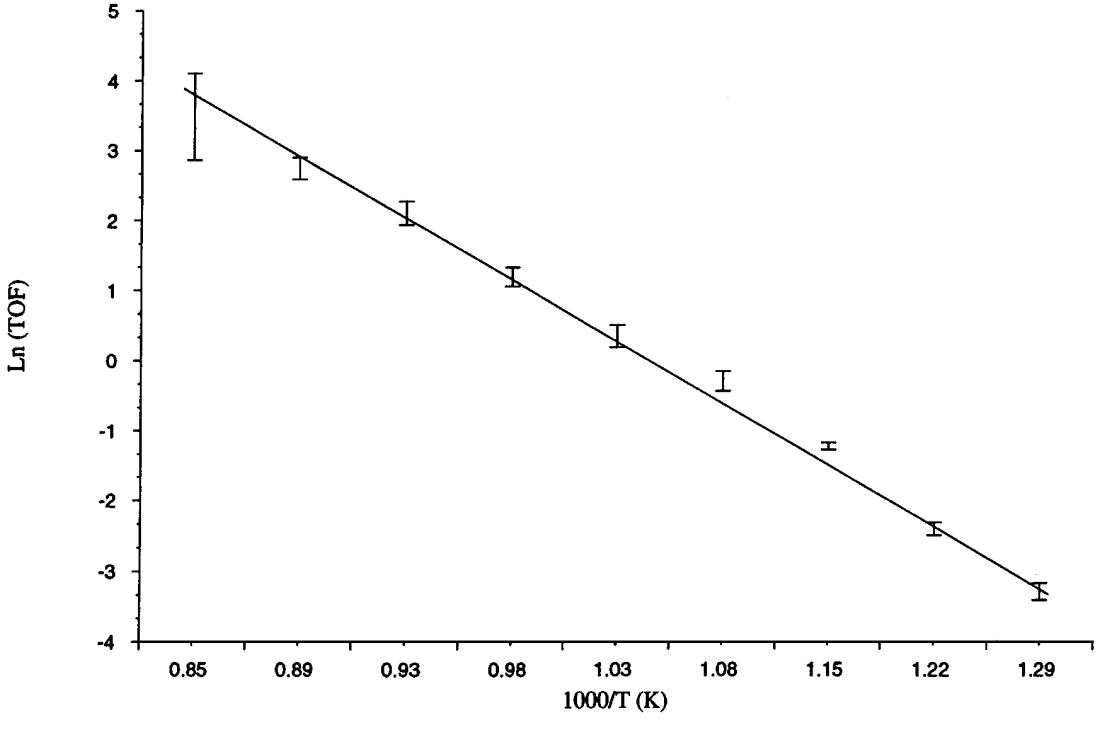

FIG. 9. Temperature dependence (Arrhenius plot) of the graphite–NO reaction using STM for the TOF (turnover frequency in 1/s) measurement of monolayer etch pits.

shows that graphite (the highest ordered form of carbon) has the lowest reactivity and the highest activation energy and that the activation energy is indeed directly related to the crystalline order of carbon material. Furthermore, this order of carbon material could be represented by the ratio of edge sites versus basal plane sites. The most important conclusion, however, is the lack of a "break" point in the Arrhenius plot and, as a result the activation energy, is relatively low, compared to the values in the literature reported on various carbons. With careful analysis of STM images, it becomes clear (as shown in Figs. 3 and 4) when the reaction temperature reaches about 700–750°C, the temperatures corresponding to the reported "break" point in the Arrhenius (53), the NO c-attack and multilayer etching become important. These processes will become increasingly important in the NO–graphite reaction as the temperature is further increased. The estimated activation energy for NO c-attack is 170 kJ/mol (35). The activation energy for multilayer etching is about 116 kJ/mol (63), which is in the same range of the activation energy of monolayer etching. In the experimental kinetic procedures reported in the literature, it is not possible to distinguish between the edge site reaction (monolayer etching), basal plane attack (c-attack), and multilayer etching. The generally observed kinetic behavior that is reported in the literature only reflects the global rates of the NO–carbon reaction, and thus it is not surprising that two temperature regimes with two activation energies and a "break" point in the Arrhenius plot are often reported. With our results, the following conclusions can be made: (a) the temperature "break" point with two temperature regimes and two activation energies for NO–carbon reaction is caused by the contribution of NO basal plane c-attack and the formation of deep pits in the high temperature regime; (b) the higher activation energies of NO c-attack, compared to the monolayer and multilayer etchings, contribute to the higher apparent activation energy as obtained in the global rate measurements for the NO–carbon reaction (53); (c) "intrinsic rate" can only be related to a certain process, i.e., either to edge site reaction or c-attack reaction or multilayer etching, since each process has a different mechanism; (d) the lower activation energy is associated with the true "intrinsic rate" of monolayer edge site only. It is worth noting that the variation in the kinetic behaviors reported from many sources (53, 54) can be attributed to the different dominating roles of the three processes above (monolayer etching, basal plane c-attack, and multilayer etching) and that the overall behavior of the actives sites could be a statistical average of the behavior of those individual processes.

Comparison of NO–Graphite Reaction to Other Reactions

Table 3 summarizes the data for graphite gasification reactions using various gases and reaction conditions. In the case of the 5% NO run, which was discussed above, the data indicates a first-order reaction with respect to NO concentration. In the low temperature range, the NO reaction has about the same reaction rate as N_2O i.e., 0.28 1/s for NO and 0.29 1/s for N_2O. Since the N_2O-carbon reaction is considered an elementary reaction, the result above implies that in this low temperature range, the NO–carbon reaction has the same rate-limiting step as N_2O–carbon does, and it might be the step of desorption of surface complexes (54, 64). However, in the high temperature range, different rates are observed, 9.98 1/s for NO and 17.3 1/s for N_2O at 800°C, indicating different rate-limiting steps for the two reactions. Since the same elementary step of the N_2O–carbon reaction no longer controls the NO–carbon reaction rate, other factors must be slowing down the NO–carbon reaction rate. There is evidence that the formation of N_2 through NO/N_2O reduction does not involve a surface nitrogen intermediate (65, 66). While N_2O can react on the surface to release N_2, the dissociation of NO should involve the coordination between two NO molecules. Therefore, instead of surface desorption, the NO coordination may play a role for the rate-limiting step at high temperatures. From Table 3, the NO–carbon and O_2–carbon reactions are first order with respect to NO or O_2 concentrations. (Fractional orders for the C–O_2 reaction are often found in the literature.) Since the TOF is ~3.5 1/s for 1% NO and ~4.5 1/s for 20% O_2, the NO–carbon reaction proceeds at least 15 times faster than the O_2–carbon reaction. Finally, the variation in the kinetic behavior for graphite samples (53) was not observed in our two totally different graphite samples. One of our graphite samples is HOPG with very high purity and the other is natural single crystal graphite from Ticonderoga, New York. The 750°C run shows almost the same TOF after accounting for different O_2 concentrations according to the first-order kinetic rule. Once again, this result is different from those reported (53), and the possible reason is our unique STM-based method for obtaining the intrinsic rate of the edge site reaction. We would expect the same nondiscretion for the NO–carbon reaction with different graphite samples by taking into account the intrinsic rate for edge site reaction.

ACKNOWLEDGMENT

This work was supported by NSF Grant CTS-9523801.

REFERENCES

1. Walker, P. L., Jr., Rusinko, F., Jr., and Austin, L. G., *in* "Advances in Catalysis," Vol. 11, p. 133. Academic Press, New York, 1959.
2. Yang, R. T., *in* "Chemistry and Physics of Carbon," Vol. 19, p. 163. Dekker, New York, 1984.
3. Laine, N. R., Vastola, F. J., and Walker, P. L., Jr., *J. Phys. Chem.* **67**, 2030 (1963).
4. Radovic, L. R., Jiang, H., and Lizzio, A. A., *Energy & Fuels* **5**, 68 (1991).
5. Huttinger, K. L., and Nill, J. S., *Carbon* **28**, 457 (1990).
6. Chen, S. G., and Yang, R. T., *J. Catal.* **141**, 102 (1993).

7. Ergun, S., and Mentser, M. R., *in* "Chemistry and Physics of Carbon," Vol. 1, p. 203. Dekker, New York, 1965.
8. Walker, P. L., Jr., Shelef, M., and Anderson, R. A., *in* "Chemistry and Physics of Carbon," Vol. 4, p. 287. Dekker, New York, 1968.
9. Baker, R. T. K., *in* "Carbon and Coal Gasification Science and Technology," NATO ASI Ser. E, Vol. 105, p. 231. Kluwer Acad., Dordrecht, 1986.
10. Floess, J. K., Longwell, J. P., and Sarofim, A. F., *Energy & Fuels* **2**, 18 (1988).
11. Kelemen, S. R., and Freund, H., *Carbon* **23**, 619 (1975).
12. Su, J. L., and Perlmutter, D. D., *AIChE J.* **31**, 1725 (1985).
13. McKee, D. W., *in* "Advances in Catalysis," Vol. 16, p. 1. Dekker, New York, 1981.
14. Thomas, J. M., *in* "Advances in Catalysis," Vol. 1, p. 120. Dekker, New York, 1965.
15. Hennig, G. R., *in* "Chemistry and Physics of Carbon," Vol. 2, p. 1. Dekker, New York, 1966.
16. Yang, R. T., and Wong, C., *Science* **214**, 437 (1981).
17. Yang, R. T., and Wong, C., *J. Chem. Phys.* **75**, 4471 (1981).
18. Yang, R. T., and Wong, C., *J. Catal.* **85**, 154 (1984).
19. Goethel, P. J., and Yang, R. T., *J. Catal.* **101**, 342 (1986).
20. Goethel, P. J., and Yang, R. T., *J. Catal.* **108**, 356 (1987).
21. Pan, Z., and Yang, R. T., *J. Catal.* **123**, 206 (1990).
22. Pan, Z., and Yang, R. T., *J. Catal.* **130**, 161 (1991).
23. Chen, S. G., and Yang, R. T., *J. Catal.* **141**, 102 (1993).
24. Chang, H., and Bard, A. J., *J. Am. Chem. Soc.* **112**, 4598 (1990).
25. Chu, X., and Schmidt, L. D., *Ind. Eng. Chem. Res.* **32**, 1359 (1993).
26. Chu, X., Schmidt, L. D., Chen, S. G., and Yang, R. T., *J. Catal.* **140**, 543 (1993).
27. Tandon, D., Hippo, E. J., Marsh, H., and Sebok, E., *Carbon* **35**, 35 (1997).
28. Hayhurst, A. N., and Lawrence, A. D., *Combust. Sci. Technol.* **18**, 529 (1992).
29. Wojtowicz, M. A., Pels, J. R., and Moulijn, J. A., *Fuel Process. Tech.* **34**, 1 (1993).
30. Ruckenstein, E., and Hu, Y. H., *Ind. Eng. Chem. Res.* **36**, 2533 (1997).
31. Chambrion, P., Suzuki, T., Zhang, Z., Kyotani, T., and Tomita, A., *Energy & Fuels* **11**, 681 (1997).
32. Garcia-Garcia, A., Chinchon-Yepes, S., Linares-Solano, A., and Salinas-Martinez de Lecea C., *Energy & Fuels* **11**, 292 (1997).
33. Shakti, G., Zhang, B., and Sarofim, A. F., *Combust. & Flame* **104**, 213 (1996).
34. DeGroot, W. F., and Richards, G. N., *Carbon* **29**, 179 (1991).
35. Chu, X., and Schmidt, L. D., *Surf. Sci.* **268**, 325 (1992).
36. Teng, H., and Suuberg, E. M., *Ind. Eng. Chem. Res.* **32**, 416 (1993).
37. Kyotani, T., Ito, K., Tomita, A., and Radovic, L. R., *AIChE J.* **42**, 2303 (1996).
38. Chen, W., and Ma, L., *AIChE J.* **42**, 1968 (1996).
39. Teng, H., Lin, H., and Hsieh, Y., *Ind. Eng. Chem. Res.* **36**, 524 (1997).
40. Teng, H., and Lin, H., *Carbon* **35**, 1811 (1997).
41. Lee, S., Permana, H., and Ng, K. Y. S., *Carbon* **32**, 145 (1994).
42. Levy, J. M., Chan, L. K., Sarofim, A. F., and Beer, J. M., *in* "Eighteenth Symposium on Combustion, 1981," p. 111.
43. Teng, H., Suuberg, E. M., and Calo, J. M., *Energy & Fuels* **6**, 398 (1992).
44. Teng, H., and Suuberg, E. M., *J. Phys. Chem.* **97**, 478 (1993).
45. Illan-Gomez, M. J., Linares-Solano, A., and Salinas-Martinez de Lecea, C., *Energy & Fuels* **7**, 146 (1993).
46. Illan-Gomez, M. J., Linares-Solano, A., Radovic, L. R., and Salinas-Martinez de Lecea, C., *Energy & Fuels* **10**, 158 (1996).
47. Suzuki, T., Kyotani, T., and Tomita, A., *Ind. Eng. Chem. Res.* **33**, 2840 (1994).
48. Yamashita, H., and Tomita, A., *Energy & Fuels* **7**, 85 (1993).
49. Richthofen, A. V., Wendel, E., and Neuschutz, D., *Fresenius J. Anal. Chem.* **346**, 261 (1993).
50. Jang, B. L., Spivey, J. J., Kung, M. C., and Kung, H. H., *Energy & Fuels* **11**, 299 (1997).
51. Marquez-Alvarez, C., Rodriguez-Ramos, I., and Guerrero-Ruiz, A., *Carbon* **34**, 1509 (1996).
52. Miettinen, H., and Abul-Milh, M., *Energy & Fuels* **10**, 421 (1996).
53. Aarna, I., and Suuberg, E. M., *Fuel* **76**, 475 (1997).
54. Li, Y. H., Lu, G. Q., and Rudolph, V., *Chem. Eng. Sci.* **53**, 1 (1998).
55. Nicolaides, R., *J. Vac. Sci. Tech. A* **6**, 445 (1988).
56. Melmed, A. J., *J. Vac. Sci. Tech. B* **9**, 601 (1991).
57. Wong, C., Yang, R. T., and Halpern, B., *J. Chem. Phys.* **78**, 3325 (1983).
58. Cen, P. L., and Yang, R. T., *Carbon* **22**, 186 (1984).
59. Strange, J. F., and Walker, P. L., Jr., *Carbon* **14**, 345 (1976).
60. Biederman, D. L., Miles, A. J., Vastola, F. J., and Walker, P. L., Jr., *Carbon* **14**, 351 (1976).
57. Yang, R. T., and Wong, C., *Science* **214**, 437 (1981).
61. Yang, R. T., and Wong, C., *J. Catal.* **82**, 245 (1983).
62. Evans, E. L., Griffiths, R. J. M., and Thomas, J. M., *Science* **171**, 174 (1971).
63. Chu, X., and Schmidt, L. D., *Carbon* **29**, 1251 (1991).
64. De Soete, G. G., *in* "5th International Workshop on Nitrous Oxide Emissions, Tsukuba, Japan, 1992."
65. Smith, R. N., Swinehart, J., and Lesnini, D., *J. Phys. Chem.* **63**, 544 (1959).
66. Orikasa, H., Suzuki, T., Kyotani, T., Tomita, A., and Martin, R. R., *in* "Proceedings, 22nd Biennial Conf. on Carbon, Amer. Carbon Soc., 1995," p. 626.
67. Moore, A. W., Highly oriented pyrolytic graphite and its intercalated compounds, *in* "Chemistry and Physics of Carbon," Vol. 17. Dekker, New York, 1981.